Copper Modified g- C_3N_4 nanosheet Prepared by Co-precipitation method enhanced Antimicrobial Applications

A. Selvam [1], M. Sheik MuhideenBadhusha[1*], R.R. Muthuchudarkodi[2], R. Marivignesh[3], S. Ramesh Kumar[4]

[1] Reg. No: 17212232032012, Research Department of Chemistry, Sadakathullah Appa College, Tirunelveli 627011 Affiliated to ManonmaniamSundaranar University, Abishekapatti, Tirunelveli 627012, Tamil Nadu, India.   selvamsophiaphd@gmail.com

[1*] Research Department of Chemistry, Sadakathullah Appa College, Tirunelveli 627011, Tamil Nadu, India.

[2] Research Department of Chemistry, V.O. Chidambaram College, Thoothukudi 628008, Tamil Nadu, India.

[3&4] Research Department of Zoology, Sadakathullah Appa College (Autonomous), Rahmath Nagar, Tirunelveli-627011 Affiliated to ManonmaniamSundaranar University, Tirunelveli, Tamilnadu, India.

Abstract:

This study used the Co-precipitation approach to successfully manufacture an effective g-C_3N_4@Cu nanocomposite. Copper nitrate was used as a source of copper, and melamine was used to create the g-C_3N_4 nanosheet. The synthesized composite was then examined under a scanning electron microscope (SEM), subjected to X-ray diffraction (XRD) studies, energy dispersive X-ray (EDX) techniques, Fourier transforms infrared spectroscopy (FT-IR), and examined using ultraviolet and visible (UV-Vis) spectroscopy by using UV-Visible absorption spectroscopy, the optical band gap of the g-C_3N_4 nanosheet and g-C_3N_4@Cu nanocomposite were determined. In comparison to the g-C_3N_4@Cu nanocomposite, the g-C_3N_4 nanosheet displayed a higher apparent absorption, and a further red shift was seen for the g-C_3N_4 containing Cu. g-C_3N_4@Cu nanocomposite was respectively 3.2 eV and 2.7 n. For g-C_3N_4, FT-IR spectra indicated a prominent peak at 840 cm-1 Additionally, a broad peak with a range of 2500 cm-1 to 3500 cm-1 provides more proof that g-C_3N_4 was constructed. A face-centered cubic (fcc) structure is visible in the g-C_3N_4@Cu Nanocomposite's X-ray Diffraction pattern. The multilayer structure and certain rods with rough areas are seen in the

1940

Eur. Chem. Bull. 2023, 12(Special Issue 4), 1940-1952

SEM picture of the g-C$_3$N$_4$ nanosheet. Additionally, the hollow sphere-like structure of the g-C$_3$N$_4$@Cu Nanocomposite is visible in the SEM image. The findings demonstrated that adding g-C$_3$N$_4$ nanosheets promotes the antibacterial properties of g-C$_3$N$_4$@Cu nanocomposite, which were created from its nucleation effect increasing the copper's surface area-to-volume ratio increasing interfacial interaction and elevating established reactive oxidative species (ROS) killing bacteria. The current study creates fresh possibilities for enhancing the antibacterial properties of biomedical polymers.

Keywords: Biomedical polymers; bandgap; nanocomposite; g-C$_3$N$_4$; SEM.

Graphical Abstract:
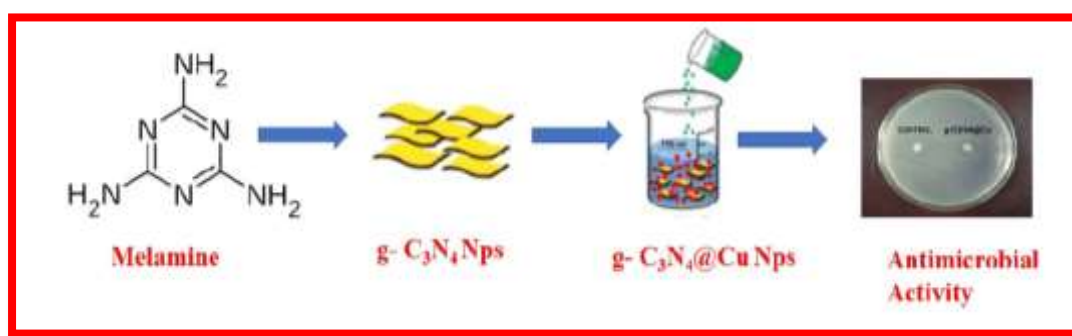
INTRODUCTION:

The bacterial illness threatens the health of people and all other living things, but it also contaminates the land, water, and environment, killing off animals and plants in the process. Antibacterial agents have thus received a lot of attention up to this point, leading to the development of numerous of them.[1] A severe public health issue has been created by the overuse of antibiotics, which has caused bacteria to develop drug resistance.[2] Recently, metal-based composites and semiconductor materials have drawn increased interest among them.[3-6] Silver,[7-8] gold,[9-10] copper,[11–12] carrollite,[13] cadmium oxide [14,] cadmium hydroxide, and zinc oxide [15–16] are just a few of the metals, metal oxides, and metal sulfide whose antibacterial characteristics have been studied thus far. As a whole, Overall, metallic structures have revealed a strong antibacterial activity [17–20] that is influenced by their size, shape, surface area to volume ratio, zeta potential, dispersion, and morphology among other factors. By raising the specific surface area to volume ratio,[21–23] the antibacterial property of nanoparticles is enhanced.[24] According to earlier research, the antibacterial function improves even at low concentrations as the aggregation of metal nanoparticles reduces.[25] It should be emphasized that microbes have no resistance to metallic particles, which speaks volumes about the value of metallic antibacterial agents. Due to its numerous uses in solar cells,[26] photocatalysis,[27] sensors,[28] and optical applications,[29] the g-C$_3$N$_4$ semiconductor has

1941

recently attracted a lot of attention Antibacterial structures [30]is another example. In addition, a variety of g-C$_3$N$_4$@Cu nanoparticle morphologies, [31] including nanotubes, nanorods, and nanoribbons [32-34],have been reported.These morphologies were created utilizing the hydrothermal and sonochemistry procedures.[35]Cu nanoparticles have significant antibacterial action, which is mostly produced by ROS.[36] Additionally, the nucleation center function of g-C$_3$N$_4$ works as a nucleation center for Cu nanoparticles, boosting their heterogeneous interfaces, which are desirable for their antibacterial properties. This makes the combination of polymer and inorganic nanoparticles appealing. It's interesting to note that putting nanoparticles into the polymer matrix changes their surface.[37] Due to its applicability in numerous sectors, including biomedical, energy, electronic, and optical, g-C$_3$N$_4$@Cu Nps has been selected as the polymeric medium in this work. The fact that this is one of More significantly, g-C$_3$N$_4$@Cu Nps has been effectively synthesized for biomedical applications with antibacterial activity against E. coli employing microwave irradiation in addition to the antibacterial features. Additionally, g-C$_3$N$_4$@Cu Nps antibacterial capabilities demonstrated overt antibacterial action against the pathogens L. monocytogenes and E. coli. The photocatalytic abilities and antibacterial activities of g-C$_3$N$_4$, which has a bandgap value of 2.7 eV, have made it one of the most intriguing materials. Current studies have demonstrated that the correct antibacterial activity of g-C$_3$N$_4$-based materials is correlated with the generation of a wide range of ROS and the simple displacement of electrons in their conduction band. According to Ding et al., Cu/protonated g-C$_3$N$_4$ composite was created by electrostatically connecting protonated g-C$_3$N$_4$ and Cu The outcomes produced are evident. Our study team published information about the g-microwave g-C$_3$N$_4$@Cu absorbing properties. The antibacterial efficacy of g-C$_3$N$_4$, Cu, and g-C$_3$N$_4$@Cu distributed in a practical matrix was examined in this study. Here, the antibacterial qualities of the Cu nanoparticles painted onto g-C$_3$N$_4$ nanosheets were meticulously examined for the first time, offering an unmatched opportunity to enhance the antibacterial properties of medicinal polymers. The outcome showed that g-C$_3$N$_4$@Cu Nps has strong antibacterial action against E. coli and S. aureus derived from the ROS generated.

MATERIALS AND METHODS

Materials

Melamine (Sigma Aldrich 99.9% purity), Copper (II) Nitrate trihydrate (Cu (NO$_3$)$_2$.3 H$_2$O), Sodium borohydride, and ethanol were purchased from Himedia, India, and were used without extra purification. All chemicals used in this examination were of analytical grade. The double distilled (DD) water was utilized in this investigation.

1942

Eur. Chem. Bull. 2023, 12(Special Issue 4), 1940-1952

Fabrication of g-C$_3$N$_4$ nanomaterial

The pure g- C$_3$N$_4$ Nanoparticle was prepared by the Hydrothermal method. Melamine was thermally treated with the muffle furnace and heated to 550°C for 4hr with a temp rate of 5°C/min.After that, the muffle furnace cooled naturally to room temperature; the product was washed with water 3 to 4 times continuously, followed by Ethanol wash three times. Then the product was dried at 60°C for 8 hrs. to obtain the resulting product of g- C$_3$N$_4$ nanoparticle. The resulting product obtained was yellow in color.

Synthesis of g-C$_3$N$_4$@Cu Nanoparticle

g-C$_3$N$_4$ @Cu nanoparticles were prepared by precipitation method.0.5 g of g- C$_3$N$_4$ was mixed with double distilled water, and 0.5mm of Cu(NO$_3$)$_2$.3 H$_2$O was added, and the reaction mass was kept under stirring for 10 hrs. at room temperature. After 10 hrs., 1.5g of sodium borohydride was added to the portion with constant stirring. The reaction temperature was elevated to 50°C, and then the precipitate was obtained because of the continuous 10 hrs.stirring. The reaction was cooled to room temperature. After cooling, the precipitate was obtained for centrifugation, followed by water and ethanol washing, and then dried for calcination. Finally,a g- C$_3$N$_4$ @Cu nanoparticle was obtained.

RESULTS

UV-vis- DRS

Figure 1 shows the UV-visible absorption spectrum that was utilized to evaluate the optical characteristics of the synthesized g-C$_3$N$_4$@Cu. The optical absorbance is influenced by the size and shape of the particles, the distance between them in the media, and the surrounding environment. For the g-C$_3$N$_4$@Cu nanoparticle, the room-temperature spectra showed string excitonic absorption peaks at 245 nm. The Tauc plot of the g-C$_3$N$_4$@Cu nanocomposite is displayed in Figure 2.
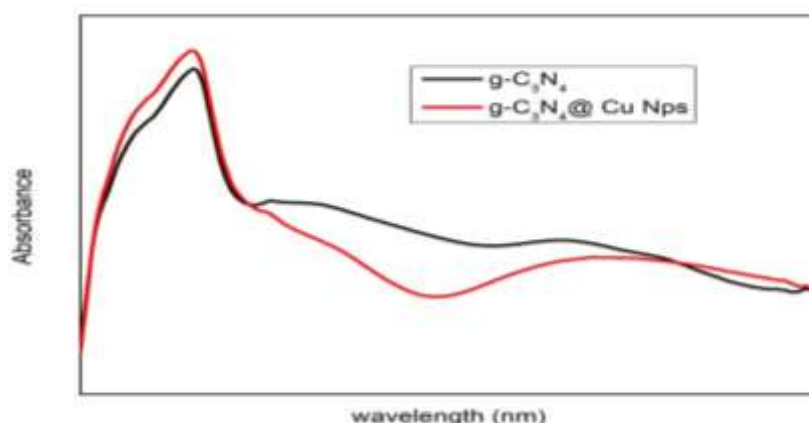

Figure 1 UV-Visible spectra of g-C$_3$N$_4$@ Cu nanoparticle

1943

Eur. Chem. Bull. 2023, 12(Special Issue 4), 1940-1952

The optical band gapof thenanoparticlesis determinedby extrapolation of the linearproofs h plots using the followingequation old equation

$$\alpha = \frac{C\,(h\upsilon - Eg^{Bulk})^2}{h\nu}$$

Where α is the absorption coefficient, hv is the photo energy, E_g is the optical band gap energy and C is the constant depending on the electron–hole mobility. Figure 2 shows the Tauc plot of the g-C₃N₄@Cu nanocomposite. The band gap energy was estimated to be about2.69 eV for g-C₃N₄@Cu nanocomposite respectively.

Where α is the absorption coefficient, hv is the photo energy, E_g is the optical band gap energy and C is the constant depending on the electron–hole mobility. Figure.2 shows the band gap energy was estimated to be about 2.69 eV for g-C₃N₄@Cu nanocomposite respectively.
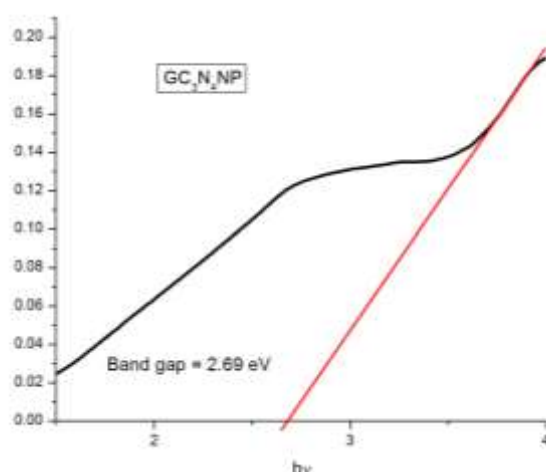

Figure2 Tauc plot g-C₃N₄@ Cu nanoparticle

FT-IR

In the FT-IR spectrum g-C₃N₄ is shown in 3. The band that appeared at the frequency range of 400-500 cm⁻¹ can be assigned to the stretching vibrational Cu band. The peaks appeared at 1383 cm⁻¹ corresponding to the stretching modes of the C-N stretching mode of g-C₃N₄. Furthermore, FT-IR spectra of g-C₃N₄@Cu shows in figure 3. The characteristic peaks appeared at 446.02, 470.56 cm⁻¹ corresponding to the stretching mode of Cu. Moreover, the peaks appeared at 1384, and 1468 cm-1 relevant to the stretching mode of C-N in g-C₃N₄. The peak at 3445.24 cm⁻¹ represents the N-H stretching mode of g- C₃N₄. Thus, the formation of g-C₃N₄ @Cu nanocomposite is confirmed by FT-IR results.
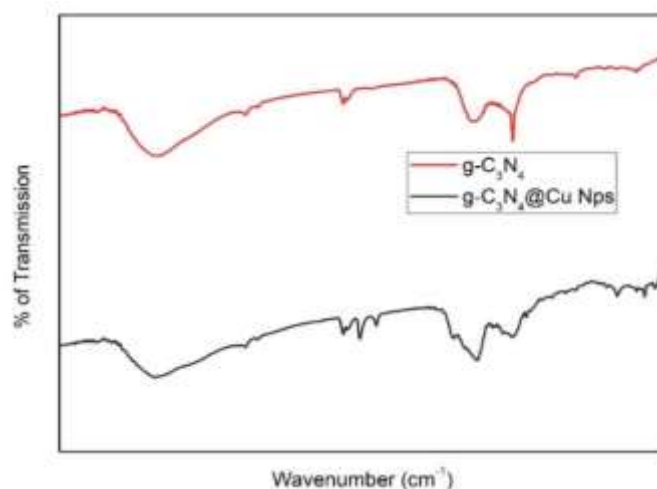
Figure 3 FT-IR Spectra of g-C₃N₄ and g-C₃N₄@Cu nanoparticles

XRD

The X-ray diffraction patterns of g-C₃N₄ and g-C₃N₄@Cu were shown in Figure 4. The diffraction peak of g-C₃N₄ (Figure 8a) at 22.3^o, 29.3^o, and 46.1^o can be assigned to (100), (002), and (103) and indexed to the hexagonal phase of g-C₃N₄. No impurity peaks were obtained in the XRD pattern of g-C₃N₄. Figure4b shows the XRD pattern of g-C₃N₄@Cu The diffraction peaks are correlated with the Cu phase, moreover, the diffraction peak appeared at 27.5^o corresponding to g-C₃N₄. This confirms the g-C₃N₄ exists on the Cu nanoparticle. Furthermore, the intensity of the XRD peaks [21]is increased while the addition of doping content. Thus, the formation of g-C₃N₄@Cu nanocomposite is confirmed. The average crystallite size is determined by Scherrer's formula given in below (equ. 1)
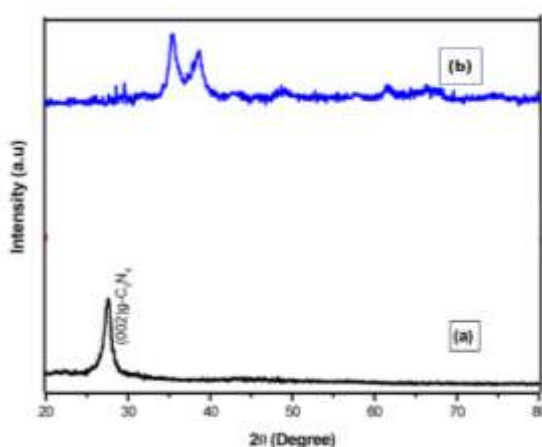

Figure 4 g-C₃N₄ and g-C₃N₄ @Cu nanoparticle

1945

Eur. Chem. Bull. 2023, 12(Special Issue 4), 1940-1952

$$D = \frac{K\lambda}{\beta \cos\theta} \quad (1)$$

Where D is the average crystallite size, β is the full-width half maximum (FWHM) of the 2θ peak. K is the shape of a factor of the particles (it equals 0.89), θ and λ are the incident of angle and wavelength of the X-rays. The crystallite sizes [22] were determined as 19.6 nm for g-C$_3$N$_4$ and 35nm for g-C$_3$N$_4$@Cu respectively. This result reveals that there is a change in crystallite size. This shows the doping effect of g- C$_3$N$_4$ on Cu nanoparticles.

Morphological study of g-C$_3$N$_4$, g-C$_3$N$_4$@Cu Nps:

The surface morphological study of g-C$_3$N$_4$and g-C$_3$N$_4$@Cu Nps was investigated through SEM analysis and shown in Figure 5. The SEM image of g-C$_3$N$_4$ shows the creation of a layered assembly and some rods with arough area. Moreover, the SEM image of g-C$_3$N$_4$@Cu Nps exhibits a hollow sphere-like structure derived from the parent Cu Nps. This implies the g-C$_3$N$_4$ doped on the surface of Cu Nps.

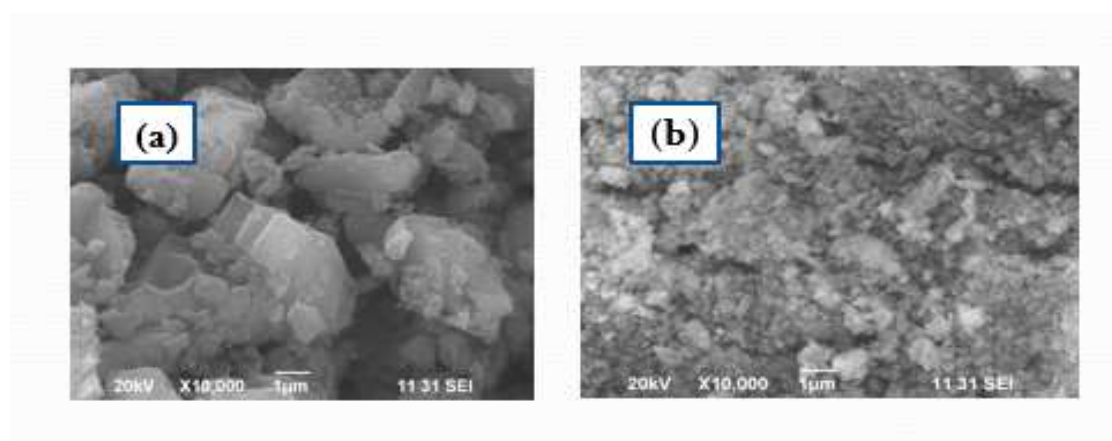**Figure 5 SEM images for (a) g-C$_3$N$_4$, (b) g-C$_3$N$_4$@Cu Nps**

HR-TEM

Figure 6 shows HR-TEM images of g-C$_3$N$_4$@Cu Nps (a-c). HRTEM images depict the emergence of nanorods. The HR-TEM images of g-C$_3$N$_4$@Cu confirmed the formation of nanorods and nanoflakes, as shown   in (Figure 6 a-c), and have good dispersion within the g-C$_3$N$_4$ matrix array. The crystalline nature of the g-C$_3$N$_4$@Cu Nps observed in the selected area diffraction pattern is shown in Figure 6d (SAED). Figure 6d illustrates the particle size distribution of g-C$_3$N$_4$@Cu Nps, the particle size was found to be 80.3 nm, which is closer to the XRD average crystallite size.
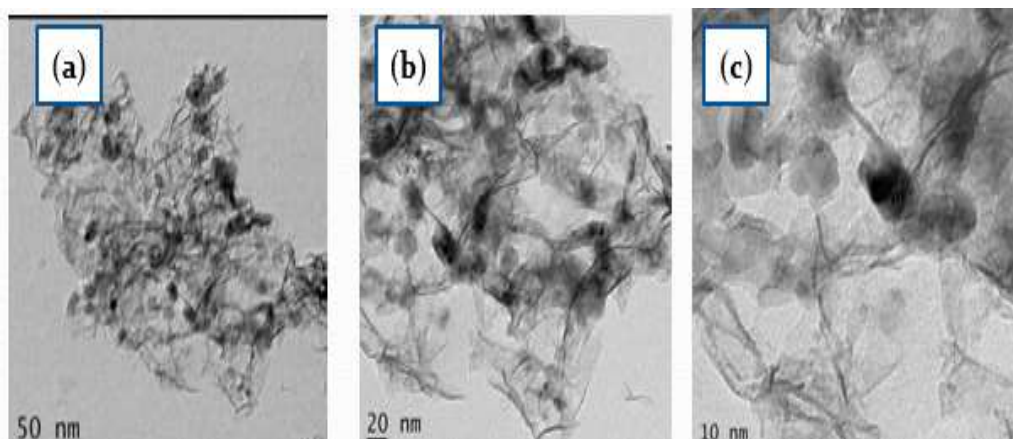
1946

Eur. Chem. Bull. 2023, 12(Special Issue 4), 1940-1952

Figure 6 HR-TEM images of g-C₃N₄@Cu Nps

DISCUSSION

The antimicrobial properties of g-C$_3$N$_4$ at a concentration of 0.1mg of 1µL against (Enterococcus faecalis, Klebsiella pneumoniae, Pseudomonas aeruginosa, and Staphylococcus aureus) have been assessed in this study. The results revealed that the g-C$_3$N$_4$ efficiently suppress pathogens' growth with variable potency. As stated in Table 1, the maximum zone of inhibition against Enterococcus faecalis (was 20mm), After that g-C$_3$N$_4$ had a zone of inhibition (16mm) against Both Klebsiella pneumonia and Pseudomonas aeruginosa, and then the minimum Zone of inhibition (14mm) against Staphylococcus aureus. The g-C$_3$N$_4$ exhibited an inhibitory effect against All four of the pathogenic strains (Enterococcus faecalis, Klebsiella pneumoniae, Pseudomonas aeruginosa, and Staphylococcus aureus).

1947

Eur. Chem. Bull. 2023, 12(Special Issue 4), 1940-1952

Table 1 Antimicrobial activity of a) *Klebsiella pneumoniae b) pseudomonas aeruginosa c)*
Staphylococcus aureus d) Enterococcus faecalis

S.NO	Figures	BACTERIAL SP	ZONE OF INHIBITION (mm)	
			control	g-C₃N₄@Cu
1		*Klebsiella pneumoniae*		16
2		*pseudomonas aeruginosa*	-	16
3		*Staphylococcus aureus*	-	14
4		*Enterococcus faecalis*	-	20

ACKNOWLEDGEMENT

ABBREVIATIONS

g- C₃N₄: Graphitic Carbon Nitride; **Nps:** Nanoparticles; **Cu:** Copper; **µL**:millionth of a liter;**mg:** Milli gram;**mm:** millimeter;**HRTEM**: High-resolution transmission electron microscopy;**SEM**:scanning electron

1948

Eur. Chem. Bull. 2023, 12(Special Issue 4), 1940-1952

microscope; **XRD:**X-Ray diffraction analysis; **UV-Vis:ultraviolet-visible; FT-IR:** Fourier-transform infrared spectroscopy; **ROS:** Reactive Oxidative Species

Reference:

1. Abbas M, Susapto HH, Hauser CA. Synthesis and organization of gold-peptide nanoparticles for catalytic activities. ACS omega. 2022;7(2):2082-90.

2. Amin Yavari S, Castenmiller SM, van Strijp JA, Croes M. Combating implant infections: shifting focus from bacteria to host. Advanced Materials2020;32(43):2002962.

3. Askari S, Halladj R. Ultrasonic pretreatment for hydrothermal synthesis of SAPO-34 nanocrystals. Ultrasonics sonochemistry. 2012 May 1;19(3):554-9.

4. Bertrand G, Filiatre C, Mahdjoub H, Foissy A, Coddet C. Influence of slurry characteristics on the morphology of spray-dried alumina powders. Journal of the European Ceramic Society. 2003;23(2):263-71.

5. Birkett M, Dover L, Cherian Lukose C, Wasy Zia A, Tambuwala MM, Serrano-Aroca Á. Recent advances in metal-based antimicrobial coatings for high-touch surfaces. International Journal of Molecular Sciences. 2022;23(3):1162.

6. Butler MS, Gigante V, Sati H, Paulin S, Al-Sulaiman L, Rex JH, Fernandes P, Arias CA, Paul M, Thwaites GE, Czaplewski L. Analysis of the clinical pipeline of treatments for drug-resistant bacterial infections: despite progress, more action is needed. Antimicrobial agents and chemotherapy. 2022;66(3):01991-21.

7. Dastjerdi R, Montazer M. A review on the application of inorganic nano-structured materials in the modification of textiles: focus on anti-microbial properties. Colloids and surfaces B: Biointerfaces. 2010;79(1):5-18.

8. Dharmalingam P, Palani G, Apsari R, Kannan K, Lakkaboyana SK, Venkateswarlu K, Kumar V, Ali Y. Synthesis of metal oxides/sulfides-based nanocomposites and their environmental applications: A review. Materials Today Sustainability. 2022; 16:100232.

9. Foresti ML, Vázquez A, Boury B. Applications of bacterial cellulose as precursor of carbon and composites with metal oxide, metal sulfide, and metal nanoparticles: A review of recent advances. Carbohydrate polymers. 2017;157:447-67.

10. Hu YH, Wang H, Hu B. Thinnest two- dimensional nanomaterial—graphene for solar energy. ChemSusChem. 2010;3(7):782-96.

1949

Eur. Chem. Bull. 2023, 12(Special Issue 4), 1940-1952

11. Jun JY, Nguyen HH, Chun HS, Kang BC, Ko S. Preparation of size-controlled bovine serum albumin (BSA) nanoparticles by a modified desolvation method. Food chemistry. 2011;127(4):1892-8.

12. Jun JY, Nguyen HH, Chun HS, Kang BC, Ko S. Preparation of size-controlled bovine serum albumin (BSA) nanoparticles by a modified desolvation method. Food chemistry. 2011;127(4):1892-8.

13. Kaur A, Preet S, Kumar V, Kumar R, Kumar R. Synergetic effect of vancomycin loaded silver nanoparticles for enhanced antibacterial activity. Colloids and Surfaces B: Biointerfaces. 2019; 176:62-9.

14. Li S, Meng Lin M, Toprak MS, Kim DK, Muhammed M. Nanocomposites of polymer and inorganic nanoparticles for optical and magnetic applications. Nano reviews. 2010;1(1):5214.

15. Lv Q, Zhang B, Xing X, Zhao Y, Cai R, Wang W, Gu Q. Biosynthesis of copper nanoparticles using Shewanellaloihica PV-4 with antibacterial activity: Novel approach and mechanisms investigation. Journal of hazardous materials. 2018;347:141-9.

16. Lyu W, Cheng Y, A J, Condorelli M, Pulvirenti M, Compagnini G, Wang X, Fu B, Scardaci V. Silver Nanoplate Composites as Nonlinear Saturable Absorbers for a Q-Switched Laser. InPhotonics 2022; 9(11): 835.

17. Mahendiran M, Mathen JJ, Racik M, Madhavan J, Raj MV. Investigation of structural, optical and electrical properties of transition metal oxide semiconductor CdOZnO nanocomposite and its effective role in the removal of water contaminants. Journal of Physics and Chemistry of Solids. 2019;126:322-34.

18. Maruthapandi M, Saravanan A, Gupta A, Luong JH, Gedanken A. Antimicrobial activities of conducting polymers and their composites. Macromol. 2022;2(1):78-99.

19. Mirzaei A, Peymanfar R, Javanshir S, Fallahi R, Karimi J. Antibacterial characteristics of CuS nanoplates anchored onto g-C3N4 nanosheets, suspended in PMMA matrix. International Journal of Nanoscience and Nanotechnology. 2021;17(4):249-60.

20. Munyai S, Hintsho-Mbita NC. Green derived metal sulphides as photocatalysts for waste water treatment. A review. Current Research in Green and Sustainable Chemistry. 2021;4:100163.

21. Pachaiappan R, Rajendran S, Show PL, Manavalan K, Naushad M. Metal/metal oxide nanocomposites for bactericidal effect: A review. Chemosphere. 2021;272:128607.

22. Palanivel B, Shkir M, Alshahrani T, Mani A. Novel NiFe2O4 deposited S-doped g-C3N4 nanorod: Visible-light-driven heterojunction for photo-Fenton like tetracycline degradation. Diamond and Related Materials. 2021; 112:108148.

23. Peng T, Li K, Zeng P, Zhang Q, Zhang X. Enhanced photocatalytic hydrogen production over graphene oxide–cadmium sulfide nanocomposite under visible light irradiation. The Journal of Physical Chemistry C. 2012;116(43):22720-6.

24. Peymanfar R, Selseleh-Zakerin E, Ahmadi A, Tavassoli SH. Architecting functionalized carbon microtube/carrollite nanocomposite demonstrating significant microwave characteristics. Scientific reports. 2021;11(1):11932.

25. Qu Q, Zeng C, Huang J, Wang M, Qi W, He Z. Cystine-assisted accumulation of gold nanoparticles on ZnO to construct a sensitive surface-enhanced Raman spectroscopy substrate. Frontiers of Chemical Science and Engineering. 2022:1-9.

26. Raha S, Ahmaruzzaman M. Facile fabrication of g-C₃N₄ supported Fe₃O₄ nanoparticles/ZnO nanorods: a superlative visible light responsive architecture for express degradation of pantoprazole. Chemical Engineering Journal. 2020; 387:123766.

27. Samsudin MF, Frebillot C, Kaddoury Y, Sufian S, Ong WJ. Bifunctional Z-Scheme Ag/AgVO3/g-C3N4 photocatalysts for expired ciprofloxacin degradation and hydrogen production from natural rainwater without using scavengers. Journal of environmental management. 2020; 270:110803.

28. Sana SS, Haldhar R, Parameswaranpillai J, Chavali M, Kim SC. Silver nanoparticles-based composite for dye removal: A comprehensive review. Cleaner Materials. 2022 25:100161.

29. Shaheen S, Saeed Z, Ahmad A, Pervaiz M, Younas U, Khan RR, Luque R, Rajendran S. Green synthesis of graphene-based metal nanocomposite for electro and photocatalytic activity; recent advancement and future prospective. Chemosphere. 2022:136982.

30. Slavin YN, Asnis J, Hńfeli UO, Bach H. Metal nanoparticles: understanding the mechanisms behind antibacterial activity. Journal of nanobiotechnology. 2017; 15:1-20.

31. Soleymani J, Hasanzadeh M, Somi MH, Shadjou N, Jouyban A. Highly sensitive and specific cytosensing of HT 29 colorectal cancer cells using folic acid functionalized-KCC-1 nanoparticles. Biosensors and Bioelectronics. 2019; 132:122-31.

32. Tavelli R, Callens M, Grootaert C, Abdallah MF, Rajkovic A. Foodborne pathogens in the plastisphere: Can microplastics in the food chain threaten microbial food safety? Trends in Food Science & Technology. 2022 Sep 6.Trends in Food Science & Technology2022; 129: 1-10.

33. Trzepieciński T, Najm SM, Pepelnjak T, Bensaid K, Szpunar M. Incremental Sheet Forming of Metal-Based Composites Used in Aviation and Automotive Applications. Journal of Composites Science. 2022;6(10):295.

34. Ye L, Cao Z, Liu X, Cui Z, Li Z, Liang Y, Zhu S, Wu S. Noble metal-based nanomaterials as antibacterial agents. Journal of Alloys and Compounds. 2022:164091.

1951

Eur. Chem. Bull. 2023, 12(Special Issue 4), 1940-1952

35. Zeng F, Huang WQ, Xiao JH, Li YY, Peng W, Hu W, Li K, Huang GF. Isotype heterojunction g-C$_3$N$_4$/g-C3N4 nanosheets as 2D support to highly dispersed 0D metal oxide nanoparticles: generalized self-assembly and its high photocatalytic activity. Journal of Physics D: Applied Physics. 2018;52(2):025501.

36. Zhang D, Yang Z, Wu Z, Dong G. Metal-organic frameworks-derived hollow zinc oxide/cobalt oxide nanoheterostructure for highly sensitive acetone sensing. Sensors and Actuators B: Chemical. 2019; 283:42-51.

37. Zhang P, He M, Huo S, Li F, Li K. Recent progress in metal-based composites toward adsorptive removal of phosphate: Mechanisms, behaviours, and prospects. Chemical Engineering Journal. 2022:137081.

1952

Eur. Chem. Bull. 2023, 12(Special Issue 4), 1940-1952